Muon g-2 Experiment

Calorimeter Calibration Report

Winnie Wang, Junior Standing
Department of Physics, University of Washington
wangw33@uw.edu

May 8th 2017

Introduction and Background

The new Muon (g-2) Experiment occurring at the Fermi National Accelerator Laboratory ("Fermilab") currently employs several calorimeters that require calibration, in order to achieve a higher precision than the last experiment at Brookhaven National Laboratory ("BNL"). As a result, improvements on the equipment and data analysis were done to maximize precision on the detection of the muon's anomalous moment.

To achieve maximum precision, the current calorimeters used in the experiment must be calibrated. The calibration of calorimeters used for the new g-2 requires that the detectors, calorimeters and calibration techniques are improved.

The current g-2 aims to calibrate the new calorimeters through simulated energy distributions based from the last g-2 experiment. The calibration procedure that is going to be used here is similar to the procedure used at BNL because the calibration must be done individually at each calorimeter. Since all 24 calorimeters are placed with different experimental machines throughout the ring, such as the trackers and kickers, these will contribute a slight change to each of the energy distributions [3]. Consequently, the calibration must be catered to each calorimeter, based on their energy distributions.

In order to maximize calibration, machine characterization and statistical analysis methods are improved from the last experiment at BNL. One of the most important improvements is done on the silicon photomultipliers, or "SiPMs", in order to increase precision in machine data. Based on the characterization of the SiPM at the Stanford Linear Accelerator Center, the SiPM was determined to be a much more precise pixel detector than calorimeters utilized in the last experiment at BNL. [2] In addition, a statistical method called the "Q-Method" significantly contributed to the precision in data analysis. By using charge as a proxy as energy, statistical precision improved significantly.

Using the SiPM characterization data obtained from SLAC and data from the last experiment, energy distributions were generated using Monte-Carlo simulation methods that were also used to simulate energy events in each calorimeter in the old g-2. Consequently, the calibration of the calorimeters is very important. To calibrate each calorimeter for the new experiment, the greatest detected energy of each calorimeter must be known.

Purpose of Analysis

To understand how well the current simulations show the greatest energy of each calorimeter, a linear regression fitting method done based on the least square regression was done to each calorimeter using ROOT, the data analysis framework. The linear fit is then applied to different fitting intervals, which are designated by setting an arbitrary maximum energy, while the initial energy is varied. Using ROOT, various energy fitting intervals were tested to see if the linear model achieves a close end fit energy.

In general, linear fitting was able to obtain results that were within ≈ 300 MeV smaller than the maximum energy of each calorimeter energy distribution, with some calorimeters in certain crystals that displayed significantly different end fit energies. Results were also able to show that the placing of the vacuum chamber causes the crystals in odd and even numbered calorimeters to differ by about 200 MeV.
In order to calibrate the calorimeters that the current g-2 is using, the calorimeters must be calibrated for inconsistencies with the current energy distributions. This is important because the trajectories that the muon goes through in the ring should be similar to that than the last g-2, since the ring magnet used in the new g-2 is the same as the old g-2 [1].

The experiment had simulated an energy distribution for all 1296 calorimeters, in order to simulate possible energy distributions of the photons that can be detected in the new 1296 calorimeters in the new g-2. The energy distributions are simulated from Monte-Carlo methods based on what was known in the last g-2. The simulations are reasonable projections of current photon distributions because chi-square testing indicated the simulations show reasonable degrees of freedom. Consequently, linear fitting methods are justified, and are used in this data analysis.

To understand the effectiveness of the simulated data, linear least squares regression fit using ROOT is done across all energy distributions to observe whether the interpolated values with the fit function would obtain the actual data. Since the energy distribution experience a linear drop after the sharp exponential drop, linear fitting is the most appropriate.

The effectiveness of the fit is then done on 4 intervals in each energy distribution, in order to see if wider fitting intervals would increase the accuracy of obtaining the fitted greatest simulated energy (or "endpoint energies") of each distribution.

Data Analysis

Across all of the distributions, each distribution displayed an exponential distribution that is simulated to have a sharp drop at around 300 MeV. After 300 MeV, the relation between photon energy and number of photon events decrease at a linear rate. This can be illuminated with an example plot from a crystal in calorimeter 8 displayed in Figures 1 and 2 (refer in the Appendix).

Using a built-in polynomial fitting function in ROOT, fits are done with a linear function, shown:

$$y = p_0 + (p_1)x \tag{1}$$

In this equation, 'y' represents the number of photons that are received per event, while 'x' represents the energies of the excited photon that the calorimeter receives. To find the fitting function for all energy distributions, the constants, p_0 and p_1, To solve for these constants, the function finds the x-coordinate where the y-intercept is zero, by assuming that the slope of the function is formed from 0 MeV to the photon with the greatest energy.

Once the linear fit is set up, ROOT will then do the fitting over 4 different energy fitting intervals. The energy intervals were obtained by varying the start fitting energy ("eStart"). The first eStart was chosen to be at ≈ 500 MeV, because the starting energy ≈ 300 MeV. The end fitting energy in each interval ("eEnd"), however, is evaluated to be at around ≈ 2600 MeV for each interval because no energy distributions had a higher energy than 2600 MeV.

The 4 intervals are then varied by adding the eStart by 200 MeV in each new interval. By adding 200 MeV to each eStart, there were 4 varieties of energy fitting intervals done, which are between 500-2600, 700-2600, 900-2600, and 1100-2600 MeVs. This is expressed from the fit graph of the same crystal in previous examples Figure 3. The four different colored plots in the graph represent the linear fit simulated based on the 4 different intervals.

Once the fit function is solved, the solved function can be used to estimate the end fitting energy of each fit. When the fit function is solved, the eEnd of each fit is interpolated by solving for the x-intercept, or the interpolated greatest energy of the solved function. After the data across all 4 fitting intervals are calculated, the data recorded, and is then plotted with respect to the eStart of each fitting interval. This is done to see the trend of the eEnd after each interval. An example plot illuminating this can be shown in Figure 5.

To further understand the energy trends in each calorimeter, the end fitted energy in a selected fitting interval (i.e. 500-2600 MeV) to observe the general trend of how much the fitted energies deviate.

In general, the trend should observe a drop in the fitted energy in the crystals across all calorimeters that are the furthest away from the muon ring, which are crystals numbered 9,18, 27, 36 and 45, because these crystals would not detect as much photons as those closer to the ring. A graph illuminating this trend is displayed in Figure 4.

Result and Discussion

By doing linear fits on all 4 intervals, it is observed that linear fitting methods are generally effective in obtaining the end fitted energy of each calorimeter because the fitted endpoint energies were close to the greatest energy of each calorimeter.

The increase in the eStart in each interval seem to have improved the end fitting energy slightly by each fitting. Each fitted endpoint energy with each fitting intervals generally approach the greatest detected energy in each calorimeter. Most crystals display this trend, like in crystal 10, and this is illuminated in Figure 7, where all 4 linear fits were almost right on top of the energy distribution. The fitted endpoint energy was also really close to the maximum energy that the energy distribution(s) had. In general, this was the case for most crystals, and they obtained linear fits that were similar to crystal 10.

However, this was not the case for crystals 8, 18, and 45 across all calorimeters. These crystals consistently showed fitted plots that deviated from this general trend observed in other crystals. These crystals were consistently observed to have larger inconsistencies in their fitted endpoint energies. In the fitted endpoint energy vs. eEnd plots of crystals 8, 18, and 45, it is consistently observed that there's a greater variation of end fit energies, which resulted a positive slope, as seen in Figures 8 through 13. Using the same calorimeters, this is observed from the fitted distribution plots of these crystals.

There are some factors that could account for this big difference in these 3 crystals. One of the main factor is the positioning of each calorimeter. Crystals that were placed furthest away from the ring magnet would not have energy distributions that are representative of the energy distribution of a crystal close to the ring.

This could potentially explain the large variations in the fitted energies in crystal 18 and 45 because both crystals (across all calorimeters) are the furthest away from ring. Since the crystal is furthest away from the ring magnet, the energy distributions are not representative of a crystal that is closer to the ring, which would receive most of the photon distribution in the calorimeter.

Another factor that can potentially influence the energy distributions is the placing of the machines throughout the magnet, such as the kickers, trackers and quads. This is important because the operation of these machines have the potential to affect the photons that travel in the calorimeters, which would affect the simulated photon distributions and affect the fitting. The material that the calorimeters are surrounded with will also affect this.

Moreover, it has recently been found that the placing of the vacuum chamber could potentially affect the energy distributions. Printing out the plot of the endpoint energy of a specific fitted interval (i.e 500-2600 MeV) showed that the energy deviations between the odd- and even- numbered calorimeters in each calorimeter deviated by $\approx$ 200 MeV. For instance, this is observed between calorimeters 10 and 11 in Figures 14 and 15, where the amplitudes of Figure 14 ranged from ≈ 1800 MeV to $\approx 2400 MeV$, whereas the amplitudes of Figure 15 ranged from ≈ 1600 to ≈ 2400 MeV.

Recent discussions had believed that this is due to the placing of the calorimeters in the vacuum chamber, and simulations had indicated that this is the case. When simulations were done without the vacuum chamber, the 200 MeV difference in fitted endpoint energies that were observed in Figures 14 and 15 were not observed. Because of this, it may have been the material that the vacuum chamber was made out of.

Conclusion

The goal of this report was to observe the quality of the simulation data, so that the current calorimeters can be calibrated based on the simulations used here. From computing least squares linear regression fit across all 1294 calorimeters, it is observed that the linear fit was able to obtain most fits across most calorimeters. However, the large deviations observed in the fits done in crystals 8, 18 and 45 may mean that these crystals need more investigation.

Their deviations indicate that their energy distributions might have been significantly affected by their position. Since crystals 18 and 45 were much farther away from the ring, their positions may have affected the energy detection. The positioning of experimental equipment, such as kickers and trackers may have also significantly affected the detection of these crystals. Recent findings also indicate that the vacuum chamber could also have affected the energy distributions across all calorimeters, as there was a consistent ≈ 200 MeV difference between odd- and even-numbered calorimeters.

References

1. Bennett et al., "Final Report of the Muon E821 Anomalous Magnetic Moment Measurement at BNL", arXiv:hep-ex/0602035v1.

2. Feinberg et al., "Studies of an array of PbF_2 Cherenkov crystals with large-area SiPM readout", Nuclear Instruments and Methods in Physics Research A (2015).

3. Hertzog, David. "Calo Energy Calibration 2.0"

Appendix

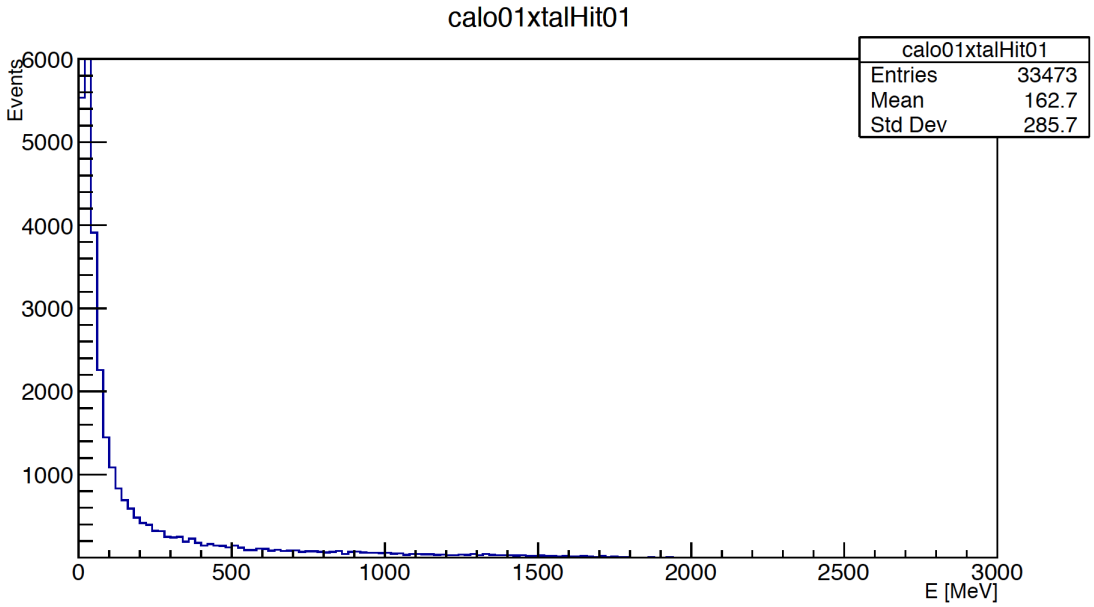

Figure 1: *An energy distribution plot of crystal 1 in calorimeter 1.*

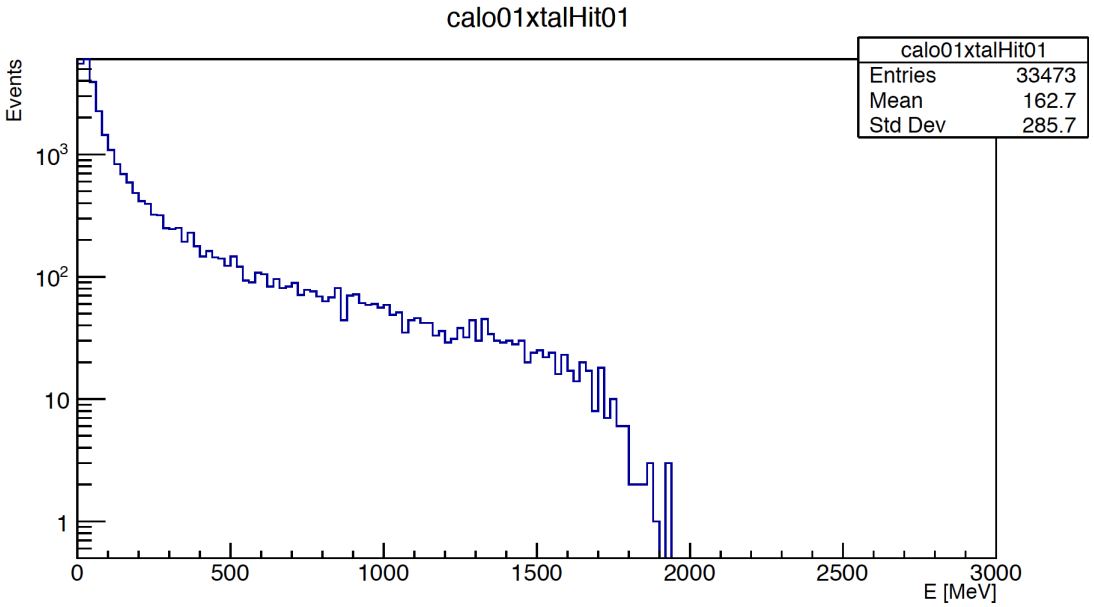

Figure 2: *An energy distribution plot of crystal 1 in calorimeter 1 at logarithmic scale.*

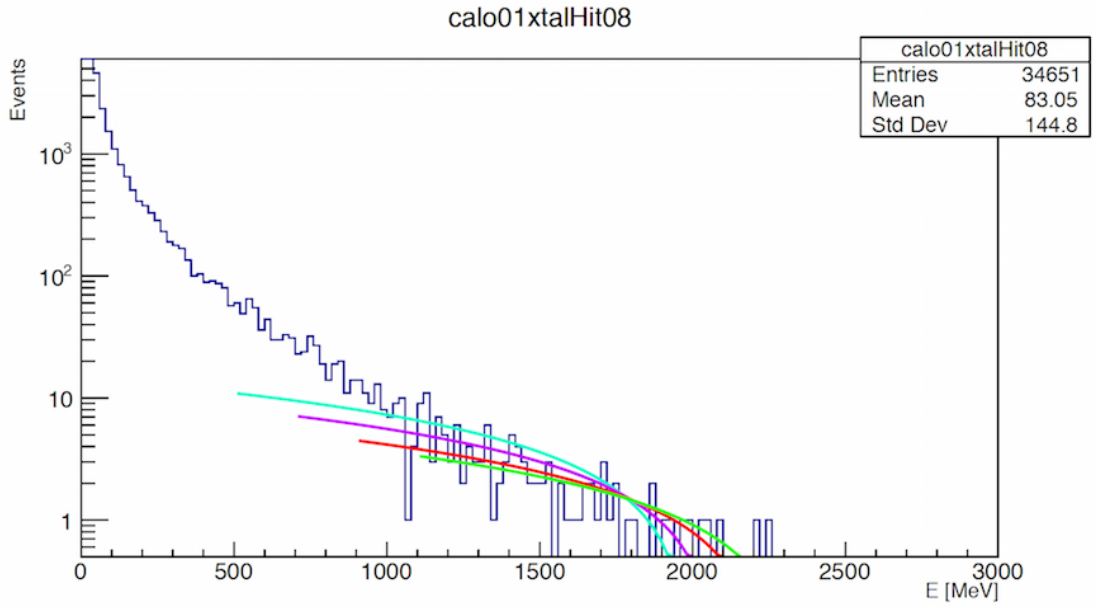

Figure 3: *An energy distribution plot with the 4 fitted plots in it. In the plot above, there are fitted energy distribution plot with 4 different fit lines of crystal 8 in calorimeter 1. Four fitting functions are displayed distinctly with different colors. Each of the 4 colors represent a fitting function done on a specific energy fitting interval. The cyan-colored fitting plot represent the linear fit between 500-2600 MeV, while the purple-colored fit represent 700-2600 MeV, red-colored fit represent 900-2600 MeV, and the green-colored fit represent the 1100-2600 MeV.*

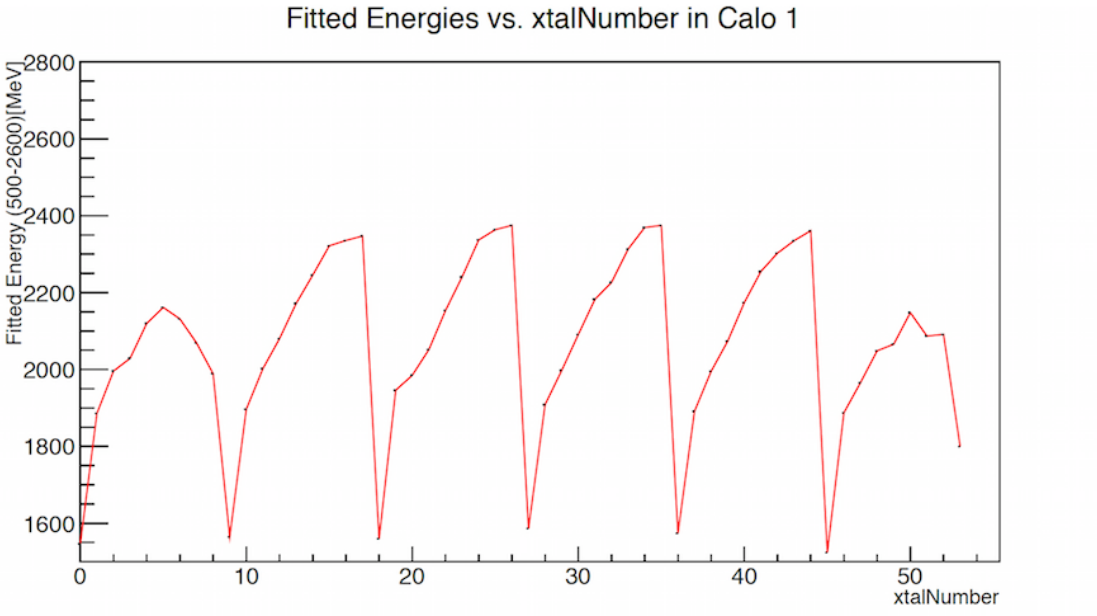

Figure 4: *Plot of end fitted energy vs. crystal number in a Calorimeter.*

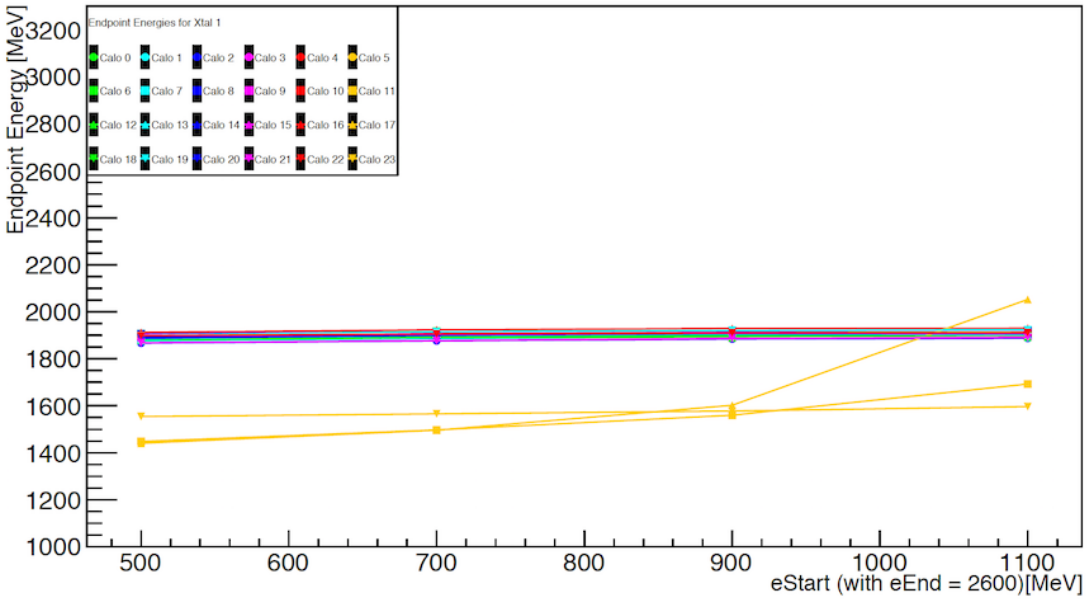

Figure 5: *Plots of fitted endpoint energy vs. eStart based on crystal 1 on all 24 calorimeters. The plot displays the 4 points of fitted endpoint energies based on the fitting results of each energy fitting interval made by changing the eStart. Consequently, there are 4 points representing the eStart of each energy interval. There are 24 separate plots representing the fitted plot of crystal 1 of each calorimeter over the 4 different intervals.*

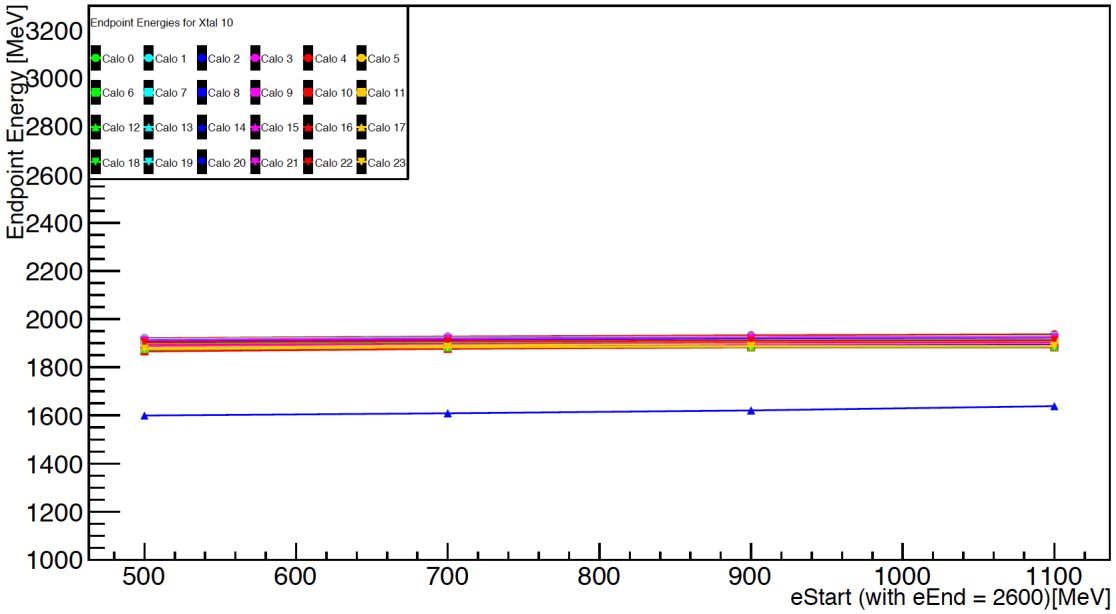

Figure 6: *Plot of fitted endpoint energies vs. eStart of Crystal 10*

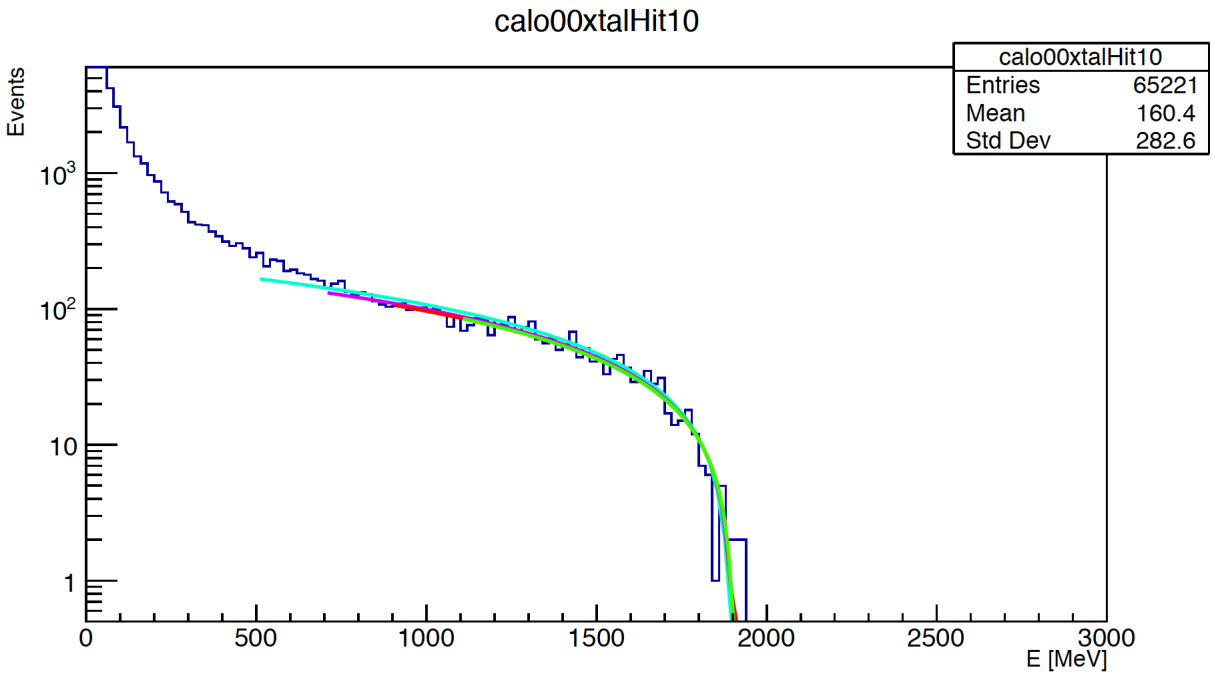

Figure 7: *Fitted energy distribution of Crystal 10 in Calo 0*

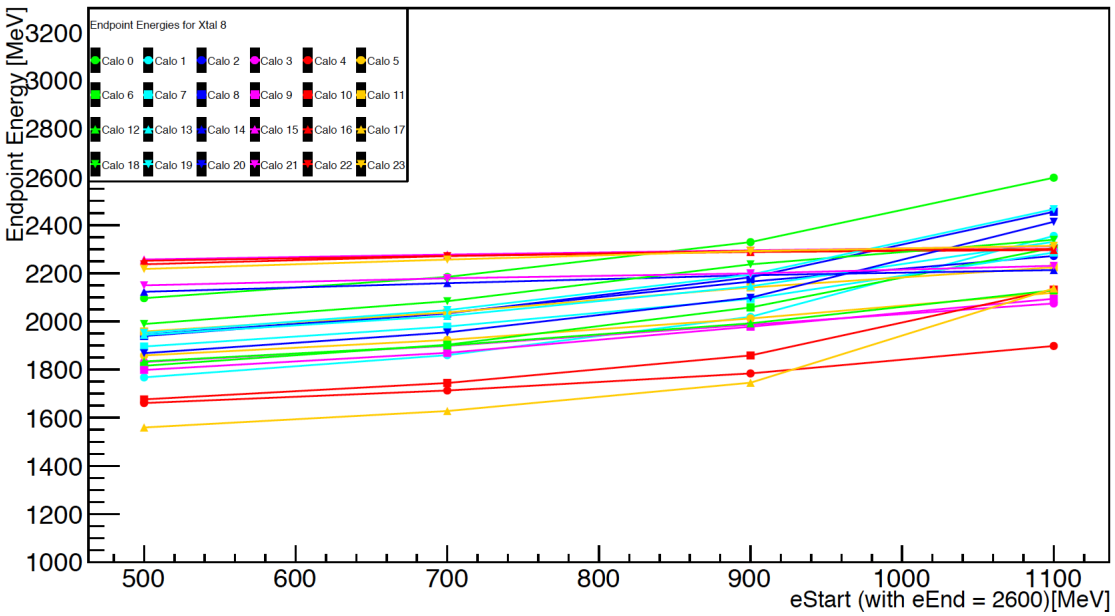

Figure 8: *Plot of fitted endpoint energies vs. eStart of Crystal 8*

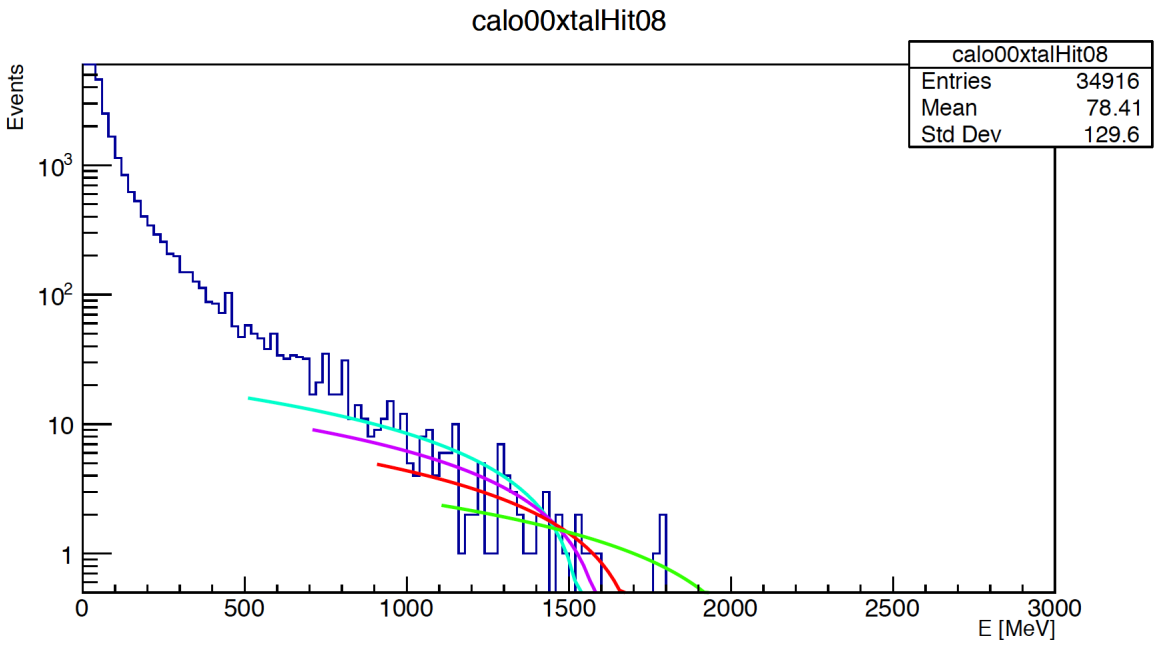

Figure 9: *Fitted energy distribution of Crystal 8 in Calo 0*

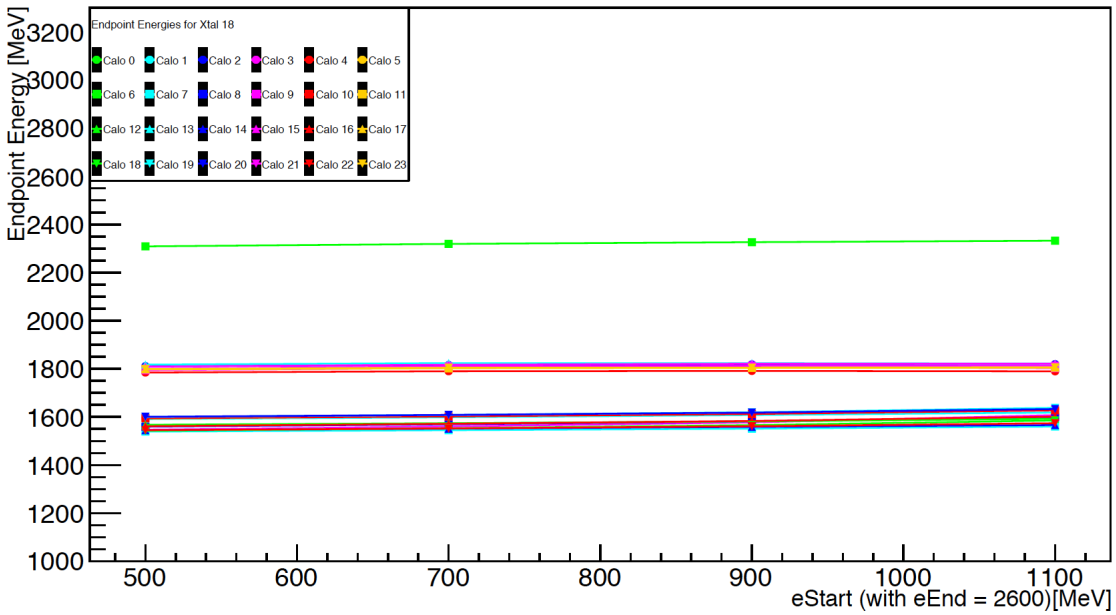

Figure 10: *Plot of fitted endpoint energies vs. eStart of Crystal 18*

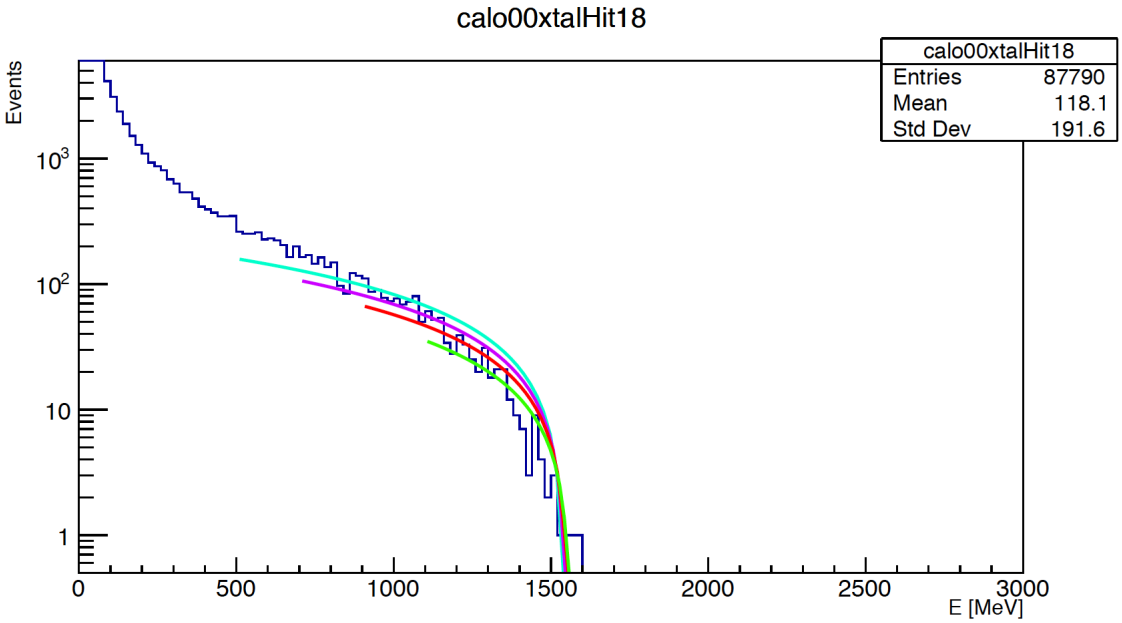

Figure 11: *Fitted energy distribution of Crystal 18 in Calo 0*

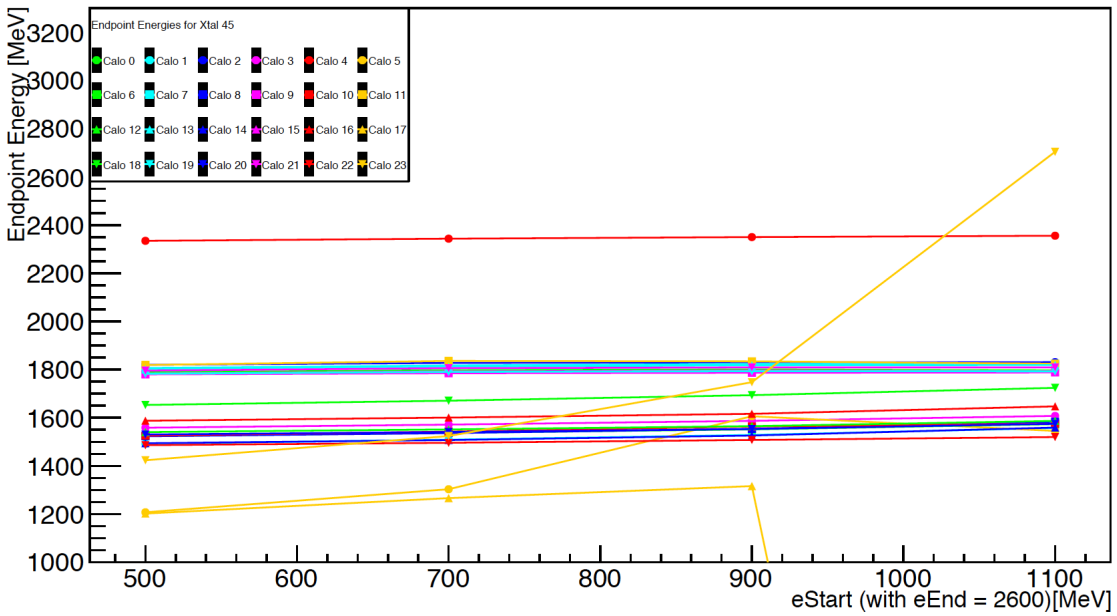

Figure 12: *Fitted energy distribution of Crystal 45*

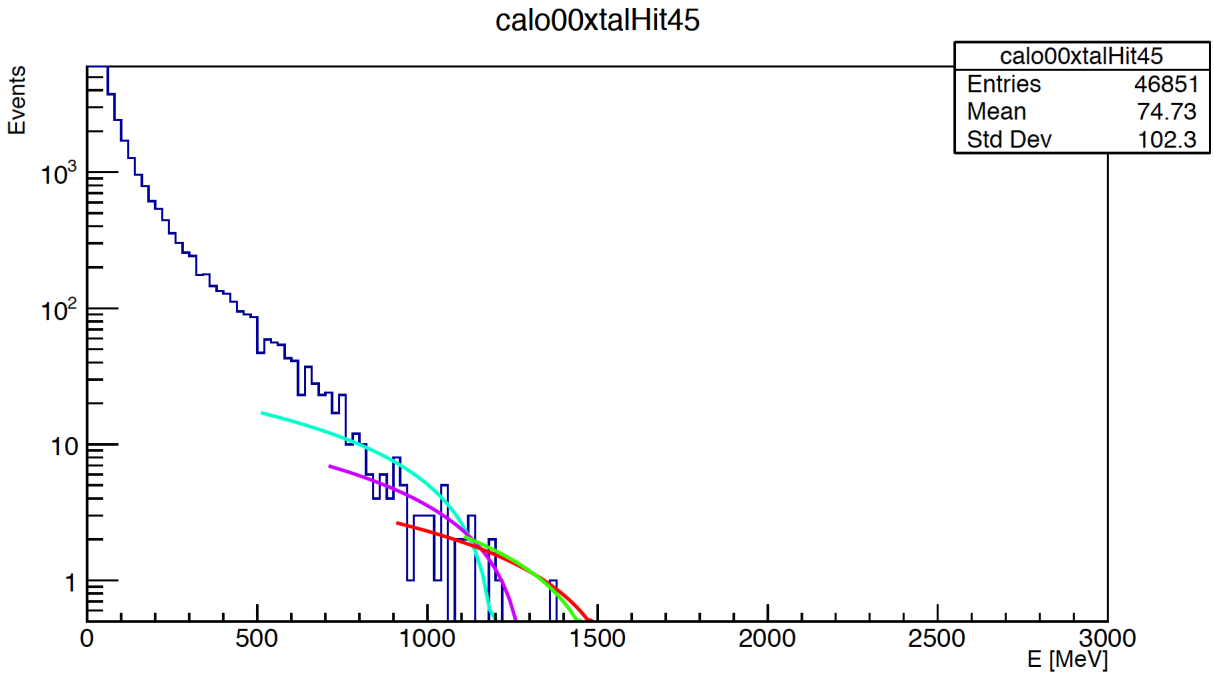

Figure 13: *Fitted energy distribution of Crystal 47 in Calo 0*

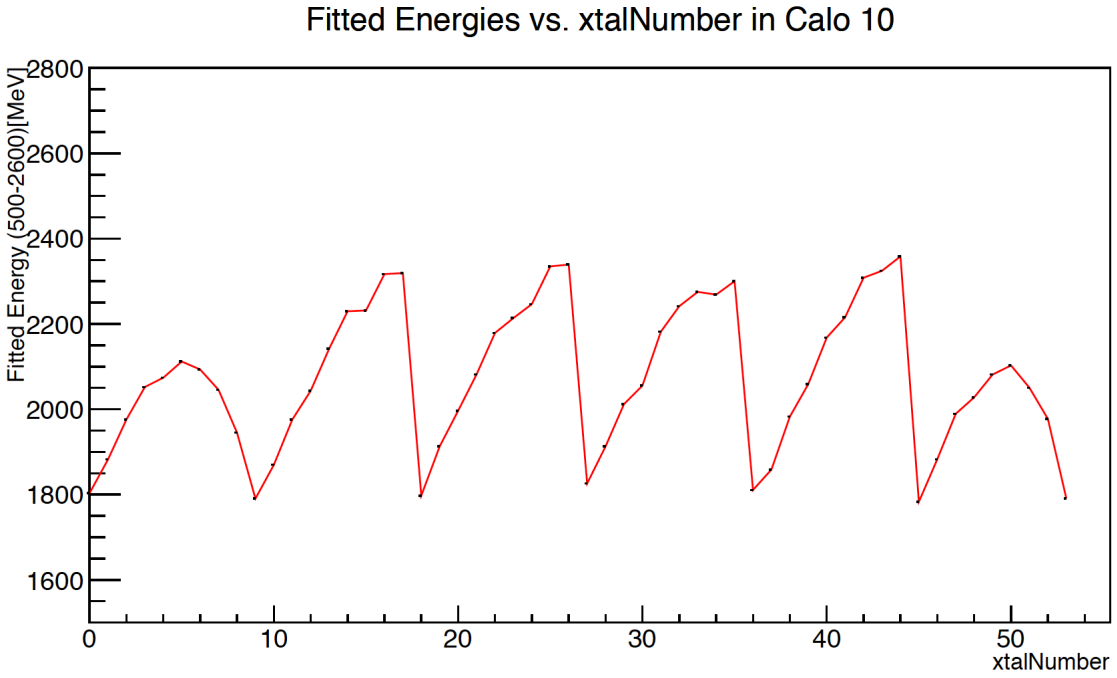

Figure 14: *Plot of fitted endpoint energies vs. crystal number in a Calorimeter in Calo 10*

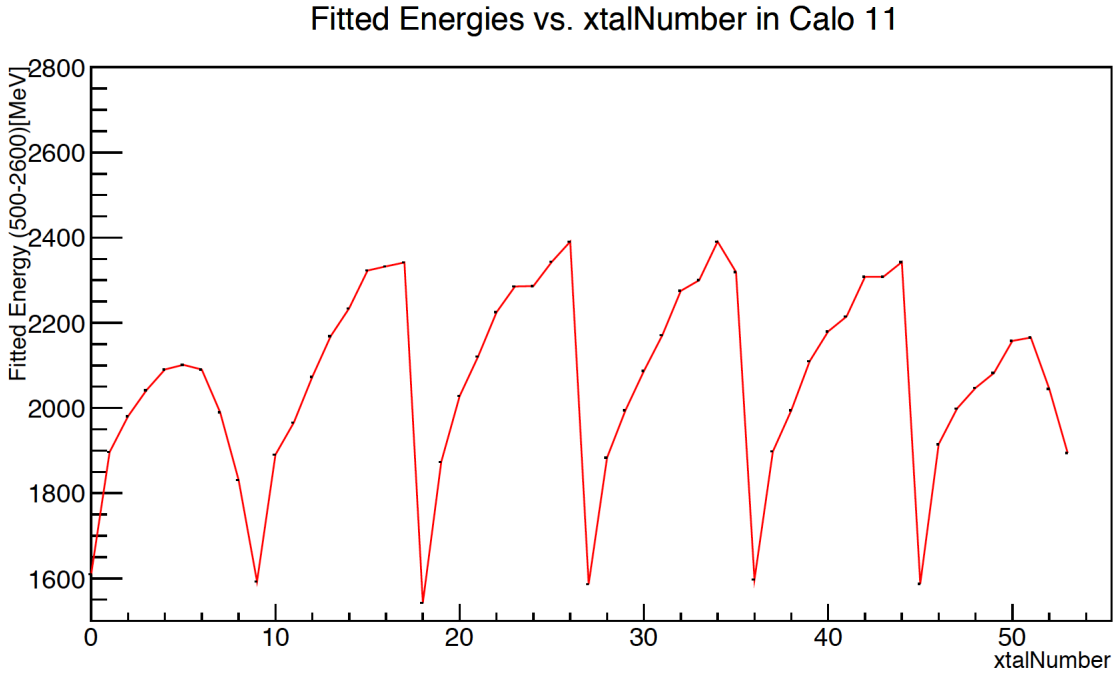

Figure 15: *Plot of fitted endpoint energues vs. crystal number in a Calorimeter in Calo 11*